ACS APPLIED MATERIALS & INTERFACES

Research Article

www.acsami.org

Mechanically Stable Thermally Crosslinked Poly(acrylic acid)/Reduced Graphene Oxide Aerogels

Heonjoo Ha,[†] Kadhiravan Shanmuganathan,[‡] and Christopher J. Ellison*[,†]

[†]McKetta Department of Chemical Engineering, University of Texas at Austin, Austin, Texas 78712, United States

[‡]Polymer Science and Engineering Division, CSIR-National Chemical Laboratory, Pune, Maharashtra 411008, India

Supporting Information

ABSTRACT: Graphene oxide (GO) aerogels, high porosity (>99%) low density (~3−10 mg cm^{-3}) porous materials with GO pore walls, are particularly attractive due to their lightweight, high surface area, and potential use in environmental remediation, superhydrophobic and superoleophilic materials, energy storage, etc. However, pure GO aerogels are generally weak and delicate which complicates their handling and potentially limits their commercial implementation. The focus of this work was to synthesize highly elastic, mechanically stable aerogels that are robust and easy to handle without substantially sacrificing their high porosity or low density. To overcome this challenge, a small amount of readily available and thermally cross-linkable poly(acrylic acid) (PAA) was intermixed with GO to enhance the mechanical integrity of the aerogel without disrupting other desirable characteristic properties. This method is a simple straightforward procedure that does not include multistep or complicated chemical reactions, and it produces aerogels with mass densities of about 4−6 mg cm^{-3} and >99.6% porosity that can reversibly support up to 10 000 times their weight with full recovery of their original volume. Finally, pressure sensing capabilities were demonstrated and their oil absorption capacities were measured to be around 120 g oil per g aerogel^{-1} which highlights their potential use in practical applications.

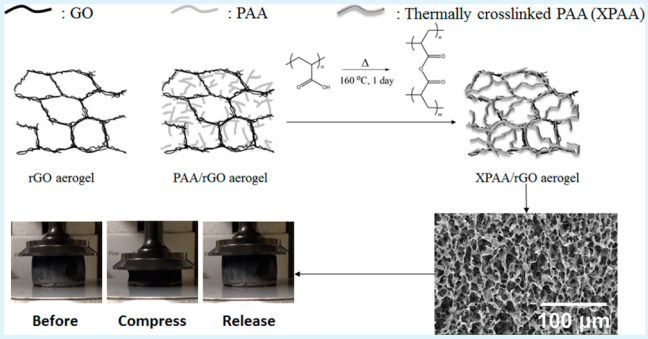

KEYWORDS: *poly(acrylic acid), graphene, aerogels, nanocomposites, environmental remediation*

1. INTRODUCTION

Graphenes are 2D sheets of carbonaceous material that possess extraordinary mechanical properties, thermal and electrical conductivities, and high surface area.[1,2] However, most of the methods that have been discovered to mass produce graphenes often require costly and tedious purification, along with associated high energy consumption, to achieve the most attractive forms of the material.[3,4] One of the solutions to reduce the cost of synthesizing graphene while preserving its excellent properties is to use a precursor such as graphene oxide (GO). GO is commonly prepared using the modified Hummers's method, which combines chemical functionalization with physical exfoliation through strong stirring or sonication of high purity graphite.[5] Through this process, the resulting GO sheets can be functionalized with numerous reactive groups including carboxylic acids, hydroxyls, and epoxides,[6,7] that can be exploited in other reactions. An often implemented additional step in the chemical processing of graphite is to reduce the GO to form a reduced GO (rGO) using chemical agents such as hydrazine,[8−10] hydriodic acid (HI),[11] ascorbic acid,[12−14] etc. These GOs and rGOs have been hypothesized as useful for many applications including energy harvesting devices, various sensors, polymer composite materials for mechanical and electrical property enhancement, etc.

Converting GOs or rGOs into a low density, highly porous cocontinuous 3D network with physical and chemical cross-links has been of significant interest for the past few years.[3,15] These high surface area materials have mass densities of ~3−10 mg cm^{-3} with porosities >99% and are usually referred as GO sponges, aerogels, or aerographites. Unfortunately, these aerogels are often found to be extremely weak and delicate to handle due to the weak van der Waals interactions between adjacent graphene sheets that leads to a brittle skeleton.[3,15] To improve the mechanical stability of the aerogel, small amounts of additives, such as carbon nanotubes (CNTs) or ethylenediamine (EDA),[16,17] which can form strong interactions with the GO sheets, have been incorporated. An alternative approach is to introduce additional chemical cross-links to the system that can effectively reinforce the mechanical properties of the delicate aerogels. However, to retain the attractive properties of GOs, it is critical to limit the amount of material added to enhance the mechanical properties of the aerogel to prevent the pore structure from collapsing or attrition of other desirable properties. Furthermore, the chemical cross-linking reactions must occur after the aerogels are formed or simultaneously

Received: January 14, 2015
Accepted: February 25, 2015
Published: February 25, 2015

DOI: 10.1021/acsami.5b00407
ACS Appl. Mater. Interfaces 2015, 7, 6220−6229

during aerogel formation, to reduce the possibility of damage or disruption of the structure of the GO aerogels.

Recently, Hong et al.,[18] successfully demonstrated a highly durable and elastic GO aerogel by taking advantage of the self-assembly of poly(vinyl alcohol) using glutaraldehyde as a chemical/covalent cross-linker for this polymer. This study achieved excellent compressibility and good performance of the aerogel as an electrochemical capacitor, which was one of the first published uses of polymers as mechanical property enhancers in GO aerogels. However, the density of their material was relatively high (~10 mg cm^{-3}) and the preparation steps accompanied several chemical reaction procedures which could complicate mass production.

Herein, we describe a new strategy to overcome the limitations of brittle GO aerogels by intermixing a small amount of readily available and thermally cross-linkable poly(acrylic acid) (PAA). This strategy is capable of greatly enhancing the mechanical properties while simultaneously maintaining all other attractive properties (i.e., high porosity, conductivity, low density, high surface area, etc.) of the GO aerogels. This is a low cost, simple and straightforward approach that does not include complicated or multistep chemical reactions. We report here the general approach that was developed, along with the effect of molecular weight and concentration of the thermally cross-linkable polymer additive, on the structure and properties of reduced GO aerogels (termed XPAA/rGO aerogels herein). We also demonstrate how the attractive properties of these mechanically robust aerogels can be useful in applications, such as superabsorbents and pressure sensors.

2. EXPERIMENTAL SECTION

2.1. Materials. PAAs with viscosity average molecular weight (M_v) of 450 000 and 1 250 000 were purchased from Sigma-Aldrich and used without any further purification. A 55% HI solution was chosen as the reducing agent for GOs and was purchased from Sigma-Aldrich. Sulfuric acid, potassium permanganate, hydrogen peroxide, and hydrochloric acid to prepare GOs were purchased from Fisher Scientific and used as-received. Preoxidized graphite from Bay Carbon Inc. (SP-1) was used to prepare GOs.

2.2. Preparation of GO. GO was synthesized according to the Hummers's method with slight modification as described in detail elsewhere.[5] Briefly, preoxidized graphite (5 g) was added to concentrated sulfuric acid (98%, 125 mL) in an ice bath. Potassium permanganate (15 g) was added slowly using a spatula with vigorous stirring of the solution. The mixture was stirred at 35 °C for 2 h. Then, deionized water (DI water, 230 mL) was carefully added using a pipet followed by terminating with DI water (700 mL) and 30% hydrogen peroxide solution (12.5 mL). Dilute hydrochloric acid solution with DI water in a volume ratio of 1:10 were used to remove residual manganese salt and excess acid products. Subsequently, the solution was washed with DI water until the pH of the rinsed water reached neutral. Finally, this solution was filtered using a vacuum assisted Büchner funnel and filtrate converted into a thick slurry of GO in water. The aqueous dispersion of GO was lyophilized under vacuum for further applications.

2.3. Preparation of PAA/GO Aerogels. The GOs to PAA ratio for all of the samples prepared in this study are represented as the relative weight percentage of PAAs to 100 parts of GOs. For example, 450 kDa/25 indicates PAA having a viscosity average molecular weight of 450 kDa was used in weight ratio of GOs to PAA as 100:25. The corresponding amount of PAAs were added to DI water (10 mL) using a 20 mL scintillation vial at room temperature for 12 h with vigorous stirring. After confirming complete dissolution of PAA in DI water, dried GOs (50 mg) were added to the solution to make a 5 mg GO ml^{-1} concentrated solution. Additional stirring using a stir bar was performed for 2 h and then solution was sonicated using a 400 W probe sonicator (Branson Digital Sonifier 450) with 10% amplitude for 10 min (24 kJ) in an ice bath. This process assisted in the complete exfoliation of GOs in DI water and homogeneously mixed GOs with PAAs throughout the solution. After sonication, the solution was transferred to a 15 mL plastic vial with wide open neck using a glass pipet and freeze-dried by immersing into liquid nitrogen for 2 min then pulling vacuum at room temperature for 48 h. The resulting aerogels were low density dark brown spongelike materials with weak mechanical properties. It is noteworthy that, if the GOs were not completely exfoliated during the sonication step and/or if the aerogels were not completely dried during the vacuum step, the aerogels displayed significant shrinkage.

2.4. Preparation of XPAA/rGO Aerogels. After obtaining PAA/GO aerogels, all of the materials were taken out of the vial and immediately placed in a glass chamber containing HI vapor at room temperature for 24 h. Reducing the GOs to rGOs changed the color of the aerogels from dark brown to metallic black. To eliminate the residual HI vapor and simultaneously thermally cross-link PAAs to poly(acrylic anhydrides) (XPAAs), aerogels were heated at 160 °C for 24 h in a vacuum oven.

2.5. Characterization of XPAA/rGO Aerogels. Thermal properties of the PAAs were characterized by differential scanning calorimetry (DSC; Mettler Toledo DSC1). Heating and cooling rates of 20 °C min^{-1} were used for all experiments, and the midpoint value during the second heating curve was taken for glass transition temperature (T_g) analysis. The chemical cross-linking reaction of PAAs was investigated using attenuated total reflection Fourier transform infrared spectroscopy (ATR-FTIR; Thermo Nicolett 6700). Scanning electron microscopy (SEM; Zeiss Supra 40 V) was used to study the morphology of the aerogels and the compression/release cycle experiments were performed using a rheometer (TA Instrument AR-2000ex). The rheometer was equipped with a Peltier plate at the bottom and 40 mm parallel plate at the top. All of the compression/release cycle experiments were performed at room temperature for 10 consecutive cycles with a compression/release speed of 1000 μm s^{-1}. It is noteworthy that, since the height of the aerogels differs slightly sample to sample, a constant starting height value of 14 000 μm was set for every experiment. After loading the sample on the Peltier plate, the sample was compressed to 14 000 μm and the normal force was zeroed to eliminate any residual stress present before actual measurements. All of the data for normal stress were recalculated using the exact diameter of the aerogels by multiplying the reported values with the area of the parallel plate and dividing by the actual area of the aerogels. GOs used in this study were further characterized using X-ray diffraction (XRD; Rigaku R-axis Spider) to determine the crystallography of the material, and X-ray photoelectron spectroscopy (XPS; Kratos) to compare the hydrophilicity of the GOs before and after reduction. CasaXPS software (v 2.3.16) was used to perform curve fitting in which a Shirley background was assumed.

The density and porosity of the aerogels were calculated according to eqs 1 and 2:

$$\varepsilon = (1 - \rho/\rho_0) \times 100 \quad (1)$$

$$\rho_0 = \rho_{0,\mathrm{PAA}} \times w_{\mathrm{PAA}} + \rho_{0,\mathrm{graphite}} \times w_{\mathrm{GO}} \quad (2)$$

where ε is percent porosity, ρ is the mass density of the aerogel sample calculated from the weight of the aerogel divided by the volume, ρ_0 is the theoretical nonporous mass density, and w is the weight fraction of each component of the material. The density for graphite and PAA was taken as 2.2 g cm^{-3} ($\rho_{0,\mathrm{graphite}}$) and 1.2 g cm^{-3} ($\rho_{0,\mathrm{PAA}}$), respectively.

Mechanical integrity was tested by holding the sample by hand and attempting to cut the sample with a razor blade and a pair of scissors; mechanically poor samples fractured in a brittle fashion while mechanically robust samples could be cleanly sectioned all the way through during cutting. Oil absorption performance was conducted by immersing a small portion of aerogel in to a large quantity of six different oils. The duration of immersion was kept to 2 min. After removing the samples from the oil, samples were gently rolled on a piece of filter paper in every direction to get rid of excess oil adhered

DOI: 10.1021/acsami.5b00407
ACS Appl. Mater. Interfaces 2015, 7, 6220−6229

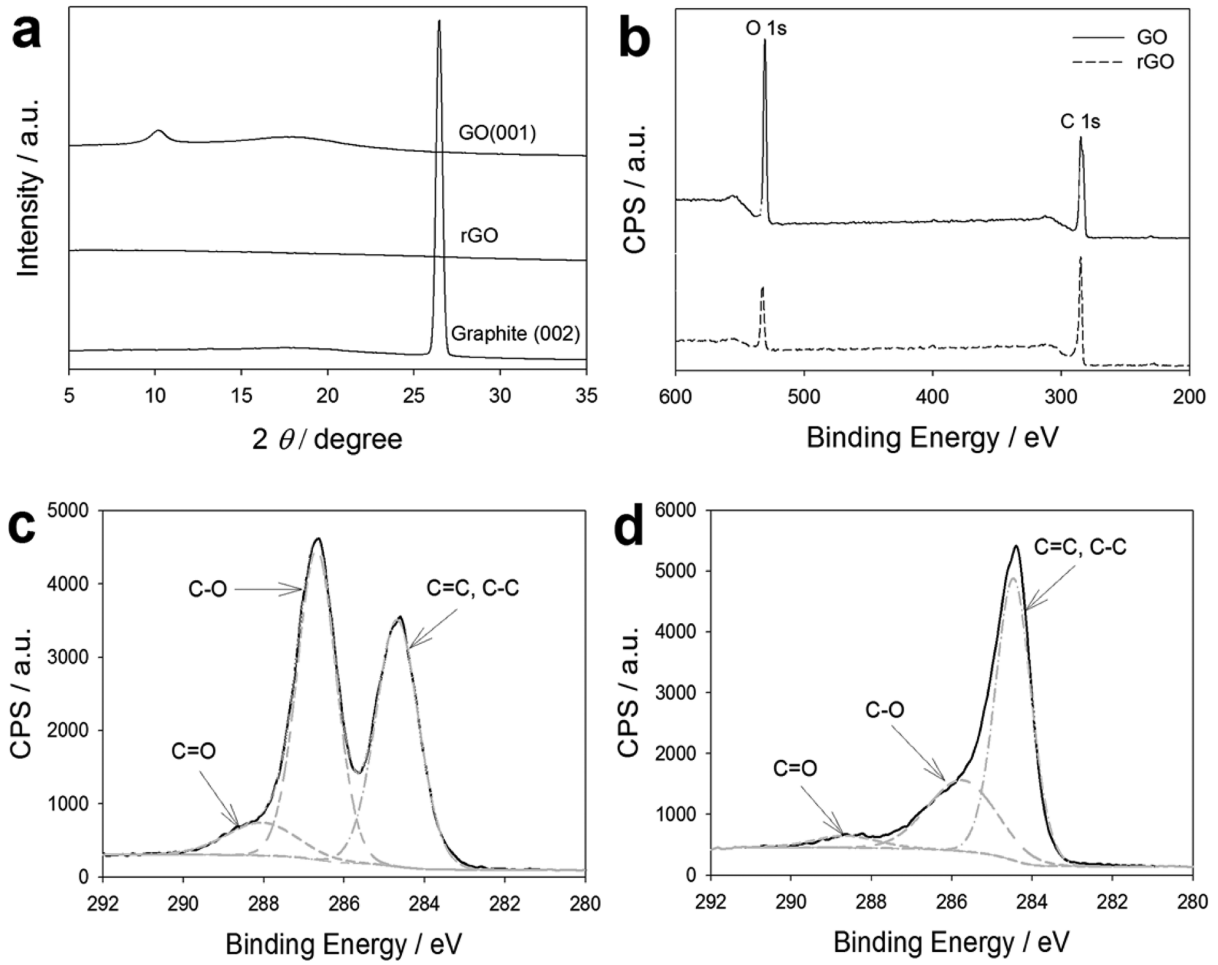

Figure 1. (a) XRD spectra of GO and rGO aerogels compared to that of preoxidized graphite. (b) XPS survey and C 1s spectra for (c) GO and (d) rGO after HI reduction and 24 h at 160 °C in vacuum.

to the surface of the aerogels. Three consecutive tests were performed and the data are presented as average values with standard deviation as the error bar. Pressure sensor performance was conducted using a LED lamp with two pieces of Cu foil as the electrodes for both ends of the aerogels. The resistivity of the material as a function of percent compressive strain was measured using a rheometer (TA Instrument AR-2000ex). A multimeter (Fluke 179 True RMS Multimeter) was used to quantitatively measure the resistivity of the material by placing two pieces of Cu foil attached to glass slides in between the parallel plates of the rheometer and the sample to be tested. The sample was squeezed to different % compressive strains while resistivity measurements were performed.

3. RESULTS AND DISCUSSION

In order to fully understand the procedures required to prepare XPAA/rGO aerogels, separate fundamental studies on reducing GO to rGO by HI vapor and thermally cross-linking PAA were first investigated.

3.1. Vapor Reduction of GO to rGO. A combination of studies of the GO and rGO aerogels (i.e., no polymer), including solubility in DI water before and after reduction, XRD spectra and XPS spectra, demonstrated the effective reducing capability of HI vapor (quantitatively by XRD and XPS in Figure 1 and qualitatively by solubility/hydrophilicity in Figure S1). XRD indicating the interlayer spacing of the GO sheets in the GO aerogel (made from freeze-drying a thick aqueous slurry of GO), rGO sheets in the rGO aerogel after HI vapor reduction followed by thermal annealing at 160 °C for 24 h, and as-received preoxidized graphite are compared in Figure 1a. The GO aerogel and graphite showed an intrinsic peak of 11° (d-spacing = 8.03 Å) and 26.6° (d-spacing = 3.45 Å), respectively, while the rGO aerogel did not exhibit any peaks.[17] This provides clear evidence that GO could be effectively reduced to rGO by using HI vapor as the reducing agent. Unlike the hydrothermal method that employs high temperature reduction (often autoclave assisted) in an aqueous environment,[19] introducing vapor phase reducing agents at ambient pressure can prevent rGOs from restacking through capillary forces and structural mobility facilitated by surrounding water. Notably, reduction of GO to rGO also results in formation of strong π electron interactions between sheets during/following the reduction step that can play an important role in the final structure and mass density of the aerogel.

Furthermore, XPS survey and C 1s spectra peaks show that the oxygen containing groups have been mostly removed by HI vapor (Figure 1b–d). The main oxygen containing components of GO arising from C═O (288.1 eV) and C–O (286.7 eV) groups are significantly reduced, while C═C, C–C (286.4 eV) becomes dominant in rGO, as shown by one single peak with a shoulder at higher binding energy (comparing Figure 1c and d). Given that a small portion of C═O and C–O groups from GO still remain after the reduction step, it is postulated that these residual functional groups (e.g., acid, hydroxyl or epoxide) could allow PAAs to form hydrogen bonds or even covalent

DOI: 10.1021/acsami.5b00407
ACS Appl. Mater. Interfaces 2015, 7, 6220–6229

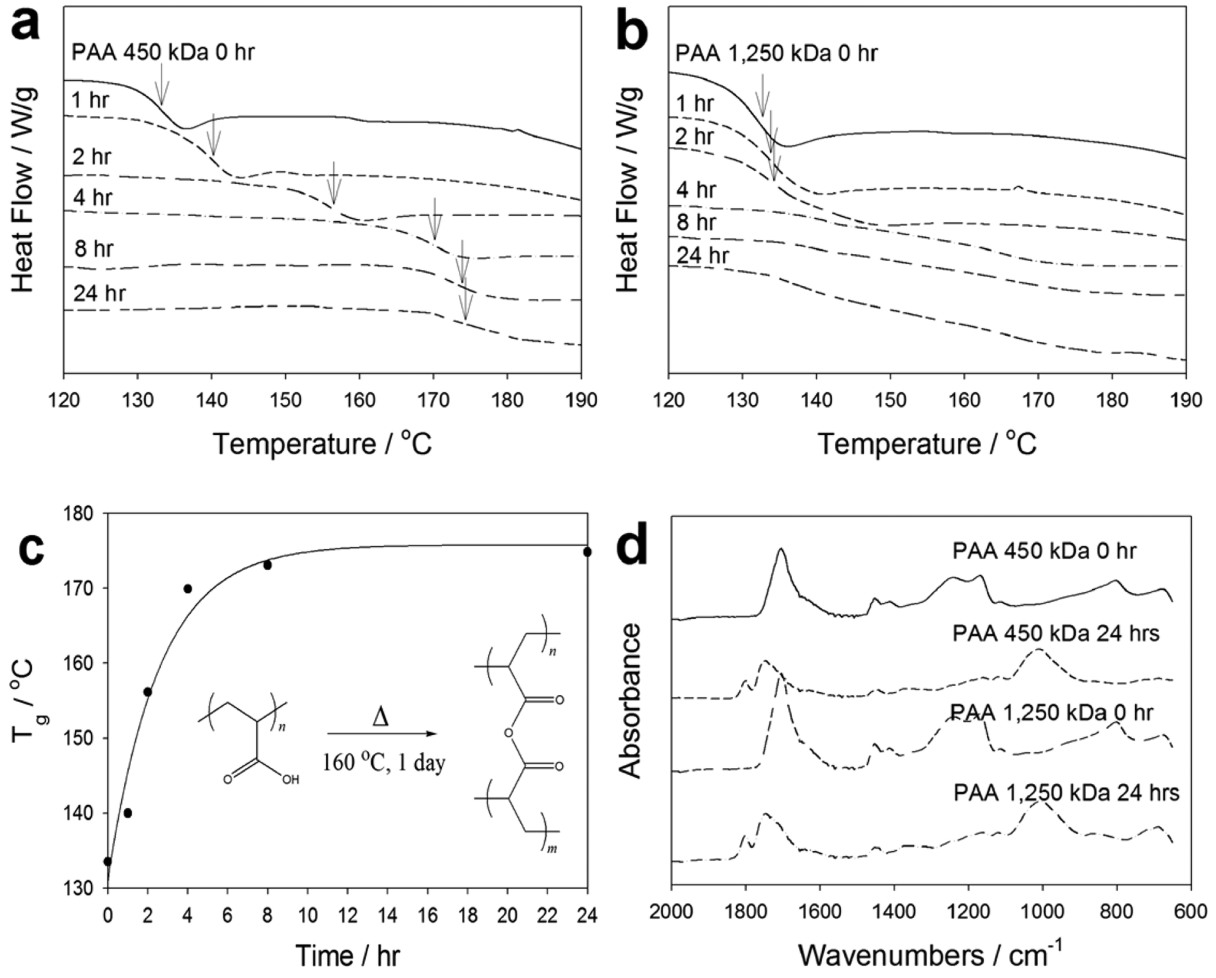

Figure 2. DSC curves indicating T_g (arrows) for PAA with M_v of (a) 450 kDa and (b) 1250 kDa after annealing at 160 °C under vacuum for different times. (c) T_g of 450 kDa PAA depending on the annealing time and (d) FTIR spectra before and after annealing PAA. FTIR spectra and DSC thermograms have been shifted vertically for clarity but are otherwise on the same scale.

Scheme 1. Scheme for Process of Preparing XPAA/rGO Aerogels

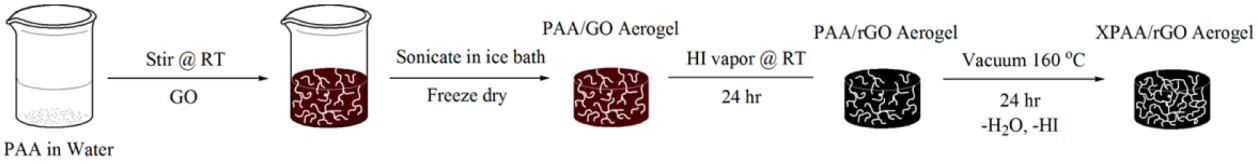

Table 1. Calculated Density and Porosity of the XPAA/rGO Aerogels and Theoretical Nonporous Density of the Precursor Mixture

sample	theoretical nonporous density ρ_0 [g cm^{-3}]	aerogel density ρ [mg cm^{-3}]	aerogel porosity ε [%]
rGO 5 mg mL^{-1}	2.20	3.67	99.8
450 kDa/25	2.00	4.38	99.8
450 kDa/50	1.87	5.08	99.7
450 kDa/75	1.77	5.48	99.7
1250 kDa/25	2.00	4.18	99.8
1250 kDa/50	1.87	5.12	99.7
1250 kDa/75	1.77	6.69	99.6

bonds with the rGO sheets during subsequent thermal annealing steps. By performing simple water solubility experiments of GO and rGO aerogels (Figure S1), hydrophilicity of these aerogels were changed dramatically after reduction, which is in good agreement with the XPS and XRD data in Figure 1.

3.2. Crosslinking Reaction Kinetics of PAA to XPAA. It has been reported by others that adjacent carboxylic acid groups in PAA can react with each other making intermolecular and intramolecular anhydrides forming XPAA by simple heating.[20,21] In order to understand the cross-linking reaction/anhydride formation and its kinetics, two different PAAs with different molecular weights (M_v = 450 and 1250 kDa) were investigated during thermal annealing at 160 °C in a vacuum oven for up to 24 h. Figure 2 summarizes associated DSC and FTIR data. The cross-linking reactions for 450 kDa PAA were expectedly accompanied by distinctive changes in the T_g with annealing time (Figure 2a) that occurred rapidly nearing a plateau after ~8 h of annealing (thermograms shown in Figure 2c and calculated T_g values in Table S1). On the other hand, the high molecular weight 1250 kDa PAA exhibited a

DOI: 10.1021/acsami.5b00407
ACS Appl. Mater. Interfaces 2015, 7, 6220−6229

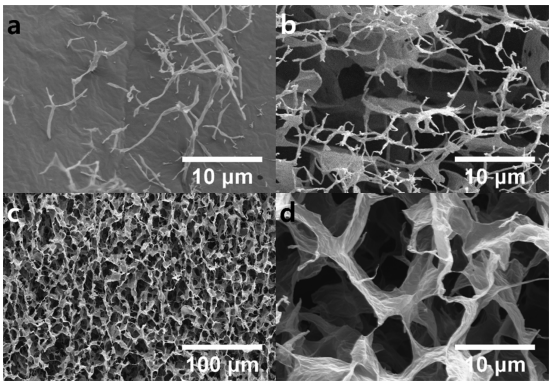

Figure 3. Selected SEM images of PAA/GO 450 kDa/50 aerogels showing (a) good interactions between PAA and GO surfaces and (b) PAA dendritic strings inside the pores before thermal annealing and corresponding XPAA/rGO aerogel after thermal annealing at (c) low and (d) high magnification.

slower reaction (as indicated by T_g) with a much broader range between T_g onset and endset (Figure 2b and Table S1), possibly due to lower polymer mobility associated with higher M_v that could slow migration of nearby acrylic acid groups.

Although the reaction conversion kinetics for PAA can be determined indirectly by DSC, absorbance spectra obtained using FTIR are far more indicative of the chemical changes. As illustrated in Figure 2d, 450 and 1250 kDa PAA both exhibited characteristic peaks of PAA, as expected. Before annealing, peaks associated with carboxylic acid pendent groups, that is, C═O stretching and C−O stretching coupled with O−H bending, were each assigned at 1703 and 1150−1300 cm^{-1}, respectively. However, after annealing PAA at 160 °C for 24 h, the position for the carbonyl group (C═O) was broadened and shifted to a higher frequency by ∼45 cm^{-1}, while C−O stretching shifted to a lower frequency region at ∼900−1200 cm^{-1}. In addition, due to the formation of anhydride linkages during thermal annealing, a new peak arose at 1820 cm^{-1}, which was assigned to the in-phase C−O stretching of the anhydride.[22] Because the FTIR spectra for the 450 and 1250 kDa PAA were nearly identical after 24 h of annealing at 160 °C and the T_g was no longer evolving, it can be concluded that the reaction was essentially completed for both cases. This reaction end point is likely representative of the vanishing mobility of cross-linking reactions as the anhydride formation proceeds rather than achieving 100% anhydride.

3.3. Morphology and Properties of XPAA/rGO Aerogels. Thermally cross-linked PAA/rGO aerogels (XPAA/rGO aerogels) were prepared by a simple procedure illustrated in Scheme 1. Although mechanical properties are improved simply by adding PAA to the GO aerogel precursor, the greatest mechanical property enhancement occurred after the GOs were reduced to rGO and the PAAs were thermally cross-linked to form XPAA. As discussed earlier, HI vapor reduced a large portion of the GOs to rGOs. The later thermal annealing process under vacuum not only thermally cross-links PAAs to XPAAs but also slightly further reduced residual GOs to rGOs (data not shown). Figure S2 qualitatively demonstrates the associated changes in hydrophilicity from PAA/GO and XPAA/rGO aerogels, which shows that the hydrophilic PAA/GO aerogels were significantly swollen with water and disintegrated into pieces compared to superhydrophobic XPAA/rGO aerogels that remained intact and floating even after submersion in DI water for 24 h. This result can be explained by both the hydrophobic nature of the rGO compared with that of GO and the cross-linking of PAA. Intermediate stage PAA/rGO samples (i.e., after reduction but before thermal cross-linking) also floated and remained intact because water could not penetrate the hydrophobic rGO porous structure (not shown).

Several aspects of the overall process can affect the final material structure porosity and density. For example, the concentration of GO in DI water was fixed at 5 mg mL^{-1} to obtain a regular porous structure after freeze-drying. It has been demonstrated in previous studies[23−25] that this particular structure provides maximum load transfer and mechanical property improvements for GO aerogels; data from the present study confirms this conclusion and is shown in Figure S3. After successfully converting the PAA/GO aerogels into XPAA/rGO aerogels, the densities (∼4.38−6.69 mg cm^{-3}) and porosities (∼99.6−99.8%) of all of the samples prepared for this study demonstrated the effectiveness of the overall process, because the intrinsic low density and high porosity of the aerogels were not adversely affected in any step. It is important to note that forming pure PAA aerogels was not possible and the structures simply collapsed during freeze-drying, possibly due to the mobility of PAA chains in the presence of a good solvent (DI water). A summary of the materials densities and their porosities are listed in Table 1, as calculated from eqs 1 and 2.

One of the main reasons for using PAA as the reinforcement polymer is not only because PAA is capable of forming thermal

Scheme 2. Scheme of Proposed Morphology of the XPAA/rGO Aerogels

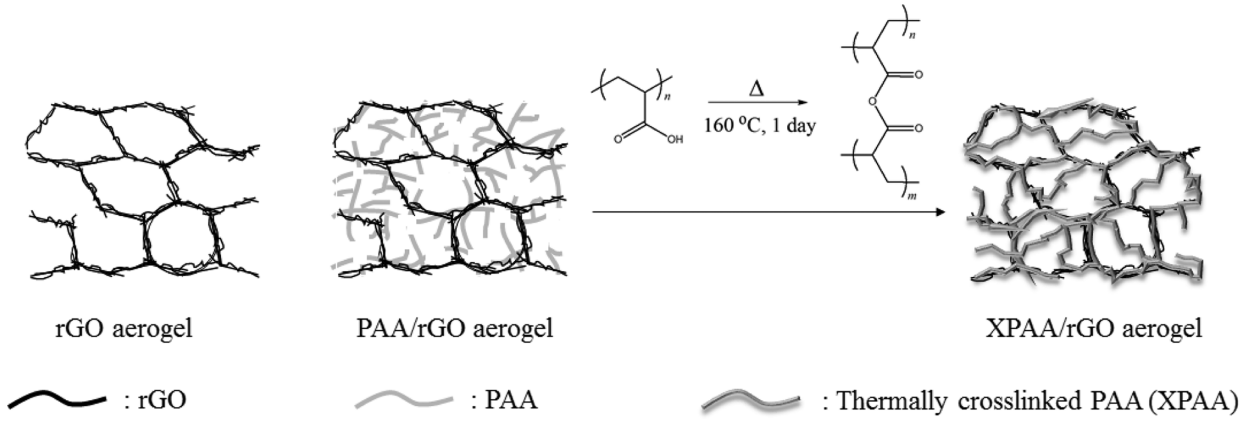

DOI: 10.1021/acsami.5b00407
ACS Appl. Mater. Interfaces 2015, 7, 6220−6229

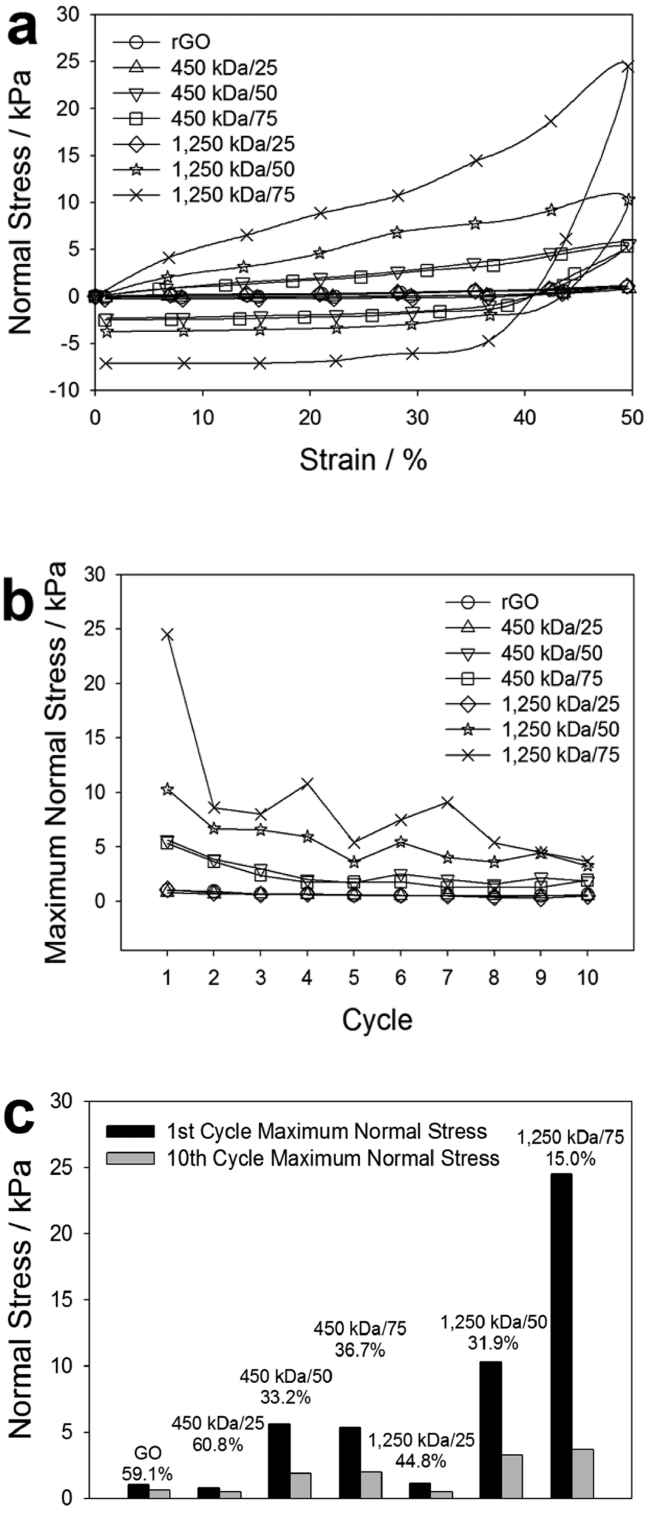

Figure 4. (a) Overlay of the 1st compression/release cycle test for strains up to 50% from XPAA/rGO aerogels with various concentrations and molecular weights of PAA. (b) Corresponding maximum normal stress values for consecutive cycles. (c) Percentage of maximum stress values remaining after 10 cycles compared to that of the 1st cycle.

cross-links in a simple thermal annealing procedure, but also because PAA can exhibit attractive interactions with GO while being completely soluble in DI water. Due to the nature of the hydrophilic carboxylic acid pendant group, PAA can form strong hydrogen bonds with carboxylic acid, hydroxyl and epoxy groups on the surface of GO sheets.[26−30] These strong interactions allowed PAA to effectively adhere to the GO surface, as shown in Figure 3a. After the PAA/GO aerogels are formed by freeze-drying, the PAAs appear to form a stringy, dendritic structure positioned within the pores and on the surface of the GO (Figure 3a and b).

Interestingly, the concentration and M_v of PAA used in the PAA/GO precursor both strongly affected the morphology of the PAA/GO aerogels. As illustrated in Figure S4, as the 450 kDa PAA concentration was increased (Figure S4a to S4c), the stringy, dendritic PAA formed more densely within the aerogel skeleton as expected, while maintaining a fairly regular pore structure. However, as the M_v increased to 1250 kDa, the PAA was not dispersing as evenly throughout the aerogels as evidenced by a less regular porous structure (representative SEM images in Figure S4d−f) with higher overall aerogel mass density (Table 1). This is possibly due to the lesser overall mobility of the high M_v polymer. Stringy, dendritic PAA was not observed in the pores at the highest PAA concentrations (Figure S4e and f). Even so, all the aerogels in Figure S4d−f still displayed significantly enhanced mechanical integrity compared to aerogels without PAA, similar to the 450 kDa samples; however, the elasticity deteriorated either due to the less regular pore structure or highly entangled polymer. These mechanical property details will be discussed in a later section.

After cross-linking PAA and reducing GO, the PAA can adhere to rGO by hydrogen bonding or covalent interactions and contribute to the enhancement in the overall stiffness and robustness by interconnecting nearby GO surfaces creating an elastic weblike structure within the porous aerogel. Interestingly, the stringy, dendritic structure of PAA evolves during thermal annealing/crosslinking to a morphology where XPAA appears mostly adhered to rGO sheets with a few XPAA bridges between sheets (Figure 3c and d). As expected, the overall properties of the final XPAA/rGO aerogels can depend strongly on the concentration and M_v of the PAA added during preparation, similar to PAA/GO aerogels. The morphologies were investigated for all of the samples (Figure S5). Identical to the PAA/GO aerogels, intermixing high concentrations of high M_v PAA tended to produce XPAA/rGOs with less regular pores and largely XPAA coated rGO sheets; therefore, the optimum concentration and M_v of PAA was found to be 450 kDa/50, 450 kDa/75, and 1250 kDa/25. Putting all this chemical and structural information together, a proposed schematic illustration of the morphology of the aerogels at different stages is presented in Scheme 2.

These morphological findings strongly correlated with the mechanical performance in compression and release cycles. As summarized in Figure 4, intermixing a small amount of PAA and thermally cross-linking the structure resulted in up to a 2400% increase in the maximum normal stress (related to compression modulus) during the first cycle (Figure 4a), whereas a maximum of 500% increase in the maximum normal stress during the 10th cycle could be achieved (summary in Figure 4b; all 10 cycles of all samples shown in Figure S6). The maximum normal stress values continuously decreased and reached an asymptotic point with increasing number of compression/release cycles (Figure 4b). The hysteresis between the first cycle and subsequent cycles can be attributed to permanent polymer and rGO structural deformation/reorganization, mainly caused during the first compression. This conclusion is supported by observing different cross-

DOI: 10.1021/acsami.5b00407
ACS Appl. Mater. Interfaces 2015, 7, 6220−6229

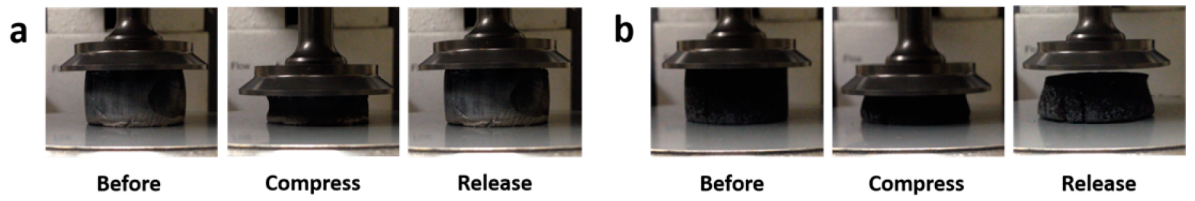

Figure 5. Digital images showing the compressibility of (a) 450 kDa/50 and (b) 1250 kDa/75 XPAA/rGO aerogels during the 10th compression/release cycle.

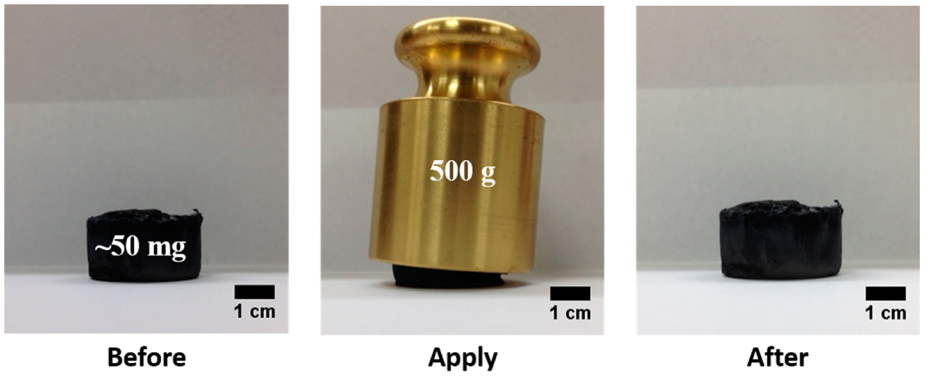

Figure 6. Images of a 450 kDa/50 XPAA/rGO aerogel before, during, and after application of a 500 g weight.

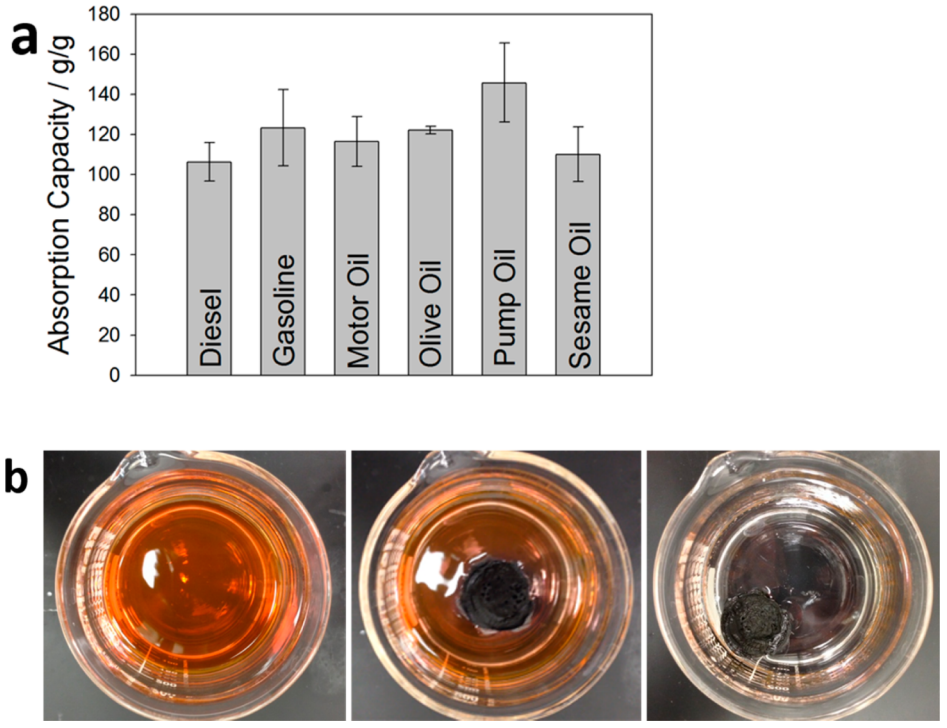

Figure 7. Oil absorption capacity comparison for different solvents. (a) Absorption capacities for various oils expressed as gram oil per gram aerogel. (b) Demonstration of oil absorption using gasoline as the absorbed solvent from t = 0 (leftmost image) to t = 35 s (rightmost image).

sectional SEM images of the compressed aerogel samples that show some fractured structural elements that appear as dangling threads (selected samples shown in Figure S7). The incorporation of a small amount of PAA for both the 450 kDa/25 and 1250 kDa/25 cases showed little or no enhancement in the maximum normal stress. However, as the concentration increased, the improvement became more pronounced (Figure 4c). Although the maximum normal stresses for all of the samples was reduced after 10 repeated cycles, most of the XPAA/rGO aerogels still exhibited much higher normal stresses compared with that of the pure rGO aerogel.

Samples such as 450 kDa/50 and 450 kDa/75 featured full recovery to the original volume after each and every compression/release cycle (Figure 5a); however, for the case of the 1250 kDa/50 and 1250 kDa/75 samples, some permanent deformation was observed with each subsequent cycle, resulting in a large permanent deformation at the end of the experiment (Figure 5b). Again, this permanent deformation

DOI: 10.1021/acsami.5b00407
ACS Appl. Mater. Interfaces 2015, 7, 6220−6229

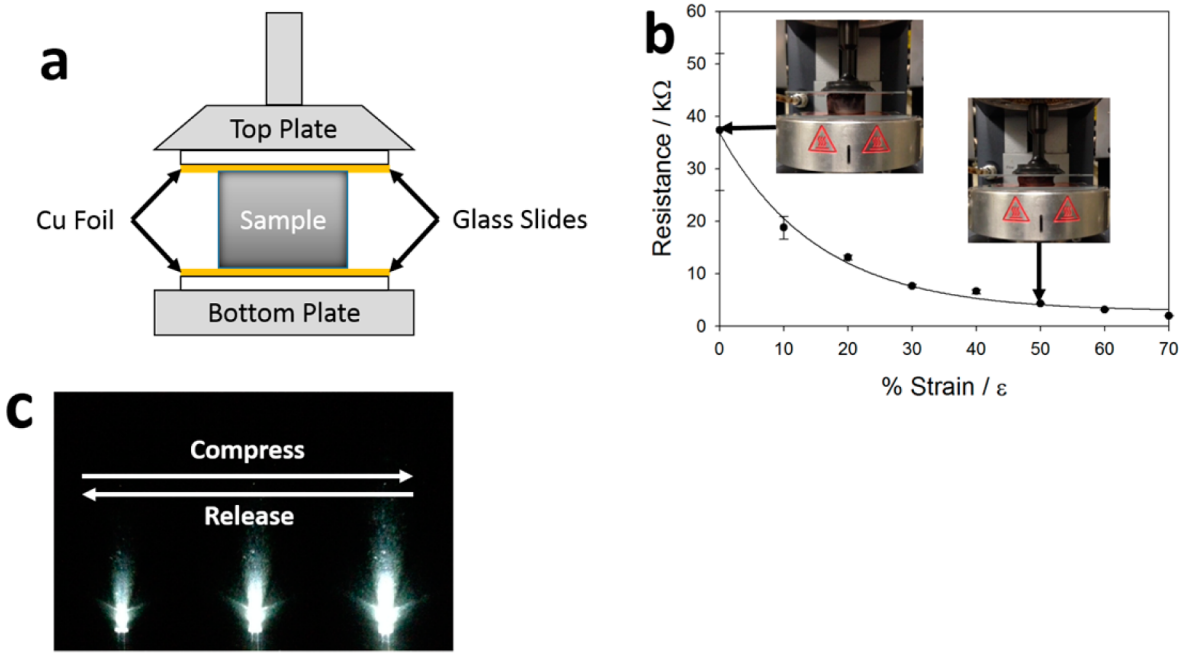

Figure 8. Pressure sensing capabilities of 450 kDa/50 XPAA/rGO through modulation of resistivity. (a) Schematic view of the experiment conducted to measure the resistivity of the material during compression between parallel plates in a rheometer. (b) Changes in resistance depending on the percent compressive strain applied. (inset) Different states in the experiments. (c) Light intensities obtained from an LED lamp in a dark room during compression and release. The light intensity varies reversibly depending on the pressure applied to the XPAA/rGO aerogels.

was strongly related to the morphological structure of these aerogels (Figure S5), where a large amount of high M_v PAA appeared to wet the GO surface instead of forming elastic bridging PAA elements as shown in Figure 3.

3.4. Applications. Despite the ultralight aspect and high surface area of rGO aerogels (without PAA) that has driven interest in various potential applications, they are typically extremely delicate and fragile, requiring careful handling to prevent them from breaking or collapsing. Practical application of these materials requires robustness during handling and deployment; therefore the qualitative mechanical integrity of the pure rGO aerogels and the XPAA/rGO aerogels was compared. Attempts to hold rGO aerogels or cut them with a razor blade or a pair of scissors were nearly impossible without significantly disrupting the original form or fracturing them completely (demonstration shown in Figure S8). However, by applying the method for forming XPAA/rGO aerogels described in this research, it was possible to firmly hold and cut aerogels cleanly without disrupting the original state of the sample (Figure S9a and b) due to the strong interactions between the rGOs and PAAs and the unique elastic crosslinked polymer structure that reinforces the aerogel. Apart from the large improvement in the handle-ability and mechanical integrity of the sample, this material features excellent recovery when subjected to a weight more than 10 000 times its own weight. Figure 6 demonstrates ~50 mg of an aerogel sample supporting a 500 g weight leading to large structural deformation. This XPAA/rGO aerogel immediately recovered back to its original state when the weight was removed without reducing the initial height or volume of the aerogel. This supporting weight ratio is equivalent to a 65 kg man holding 9 space shuttles or 125 African elephants without causing any damage. This finding was truly remarkable considering the combination of the supporting weight ratio of the XPAA/rGO aerogels and its very low density, which is nearly ~200 times lighter than water. It is noteworthy that several other studies have shown use of GO and rGO aerogels as rigid, nonelastic supports for similar weight ratios. In our view, the mechanically robust and elastic character of the XPAA/rGO aerogels, demonstrated here by their ability to support significant weight with full recovery of their original volume, highlights a new and highly attractive feature of the present materials.

To ensure that incorporating PAA did not disrupt other attractive properties of rGO aerogels, we demonstrated the performance of 450 kDa/50 XPAA/rGO aerogels as a superabsorbent and pressure sensor (superabsorbent in Figure 7 and pressure sensor in Figures 8 and S10). A series of different oils were prepared to confirm the superoleophilicity of the XPAA/rGO aerogels (Figure 7a). The average absorption capacity for six different oils was approximately 120 g oil g aerogel^{-1}, which is the range of other aerogels.[31−33] The performance of the XPAA/rGO aerogels as a superabsorbent was also visualized using gasoline colored with a fluorescent dye, which clearly demonstrated its capability as a potential material for environmental remediation (Figure 7b).

Finally, exploiting the fact that XPAA/rGO aerogels have excellent recovery after large deformation (Figure 6), this material also performed well as a pressure sensor (Figures 8 and S10). To quantitatively measure the resistance during compression, a simple experimental setup was used as shown in Figure 8a. By compressing the material, the pressure applied to the XPAA/rGO aerogels affected the number of conductive pathways, which increased the conductivity of the material. The resistance of 450 kDa/50 without compression had an average value of 37.4 kΩ and reached to an asymptotic point around ~2 kΩ when the sample was compressed over 70% (Figure 8b). This resistance range made it possible to emit light from a LED lamp with a 6 V battery using the XPAA/rGO as one element in the circuit pathway. The LED intensity increased with applied pressure/compressive strain as more conductive

DOI: 10.1021/acsami.5b00407
ACS Appl. Mater. Interfaces 2015, 7, 6220−6229

pathways were introduced, and it was completely reversible for consecutive cycles (Figure 8c).

4. CONCLUSION

By taking advantage of this process to incorporate XPAA into rGO aerogels, the delicate and fragile nature of rGO aerogels could be greatly improved. The process proposed in this work is not only simple and straightforward, but also cost-effective and does not include complicated or multistep chemical reactions. XPAA/rGO aerogels are ultralight, highly compressible and mechanically robust, due to strong interactions between rGO with PAA and the unique XPAA network morphology that reinforces the mostly rGO pore walls. Even after being subjected to a weight 10 000 times heavier than the sample, it was capable of fully recovering its original volume. In addition, the XPAA/rGO aerogels retained higher maximum normal stresses during consecutive compression and release cycles than pure rGO aerogels indicating an increased compressive modulus. The material could easily be handled and cut or trimmed without affecting other attractive properties of the aerogel. Furthermore, the performance as a superabsorbent and pressure sensor was not adversely affected by incorporation of XPAA. This approach could enable more versatile usage of graphitic aerogels in many commercial applications, such as environmental remediation, superhydrophobic and superoleophilic materials, energy storage, etc.

■ ASSOCIATED CONTENT

Ⓢ Supporting Information

Images related to the reduction process using HI vapor at room temperature, solubility comparison of GO and rGO in DI water, solubility comparison of PAA/GO and XPAA/rGO aerogels in DI water, compression test results and morphology comparisons for various concentrations of GO aerogels, cross-sectioned SEM images of freeze-dried PAA/GO aerogels before reducing or thermal annealing, cross-sectioned SEM images of freeze-dried XPAA/rGO aerogels after HI vapor reduction and thermal annealing at 160 °C for 24 h, compression−release cycle test results for all of the XPAA/rGO aerogel samples during 10 consecutive cycles, cross-sectional SEM images of XPAA/rGO aerogels taken parallel and perpendicular to the direction of compression/release after 10 cycles, mechanical integrity of pure rGO aerogels, images of the mechanical integrity and robustness of XPAA/rGO aerogels, full image of a simple circuit constructed with a LED lamp, T_g changes of PAA with different molecular weights depending on the annealing time at 160 °C. This material is available free of charge via the Internet at http://pubs.acs.org.

■ AUTHOR INFORMATION

Corresponding Author

*E-mail address: ellison@che.utexas.edu.

Author Contributions

The manuscript was written through contributions of all authors. All authors have given approval to the final version of the manuscript.

Notes

The authors declare no competing financial interest.

■ ACKNOWLEDGMENTS

Acknowledgment is made to the Donors of the American Chemical Society Petroleum Research Fund for support of this research (grant no. 53456-ND7) and the partial financial support from the Welch Foundation (grant no. F-1709). We also would like to acknowledge the Kwanjeong Educational Foundation for their financial support of H.H.

■ REFERENCES

(1) Geim, A. K.; Novoselov, K. S. The Rise of Graphene. *Nat. Mater.* **2007**, *6*, 183−191.
(2) Novoselov, K. S.; Geim, A. K.; Morozov, S. V.; Jiang, D.; Zhang, Y.; Dubonos, S. V.; Grigorieva, I. V.; Firsov, A. A. Electric Field Effect in Atomically Thin Carbon Films. *Science* **2004**, *306*, 666−669.
(3) Chabot, V.; Higgins, D.; Yu, A.; Xiao, X.; Chena, Z.; Zhang, J. A Review of Graphene and Graphene Oxide Sponge: Material Synthesis and Applications to Energy and the Environment. *Energy Environ. Sci.* **2014**, *7*, 1564−1596.
(4) Kim, K. S.; Zhao, Y.; Jang, H.; Lee, S. Y.; Kim, J. M.; Kim, K. S.; Ahn, J. H.; Kim, P.; Choi, J.; Hong, B. H. Large-Scale Pattern Growth of Graphene Films for Stretchable Transparent Electrodes. *Nature* **2009**, *457*, 706−710.
(5) Hummers, W. S., Jr.; Offeman, R. E. Preparation of Graphitic Oxide. *J. Am. Chem. Soc.* **1958**, *80*, 1339−1339.
(6) Dreyer, D. R.; Park, S.; Bielawski, C. W.; Ruoff, R. S. The Chemistry of Graphene Oxide. *Chem. Soc. Rev.* **2010**, *39*, 228−240.
(7) Kim, H.; Abdala, A. A.; Macosko, C. Graphene/Polymer Nanocomposites. *Macromolecules* **2010**, *43*, 6515−6530.
(8) Yang, D.; Velamakanni, A.; Bozoklu, G.; Park, S.; Stoller, M.; Piner, R. D.; Stankovich, S.; Jung, I.; Field, D. A.; Ventrice, C. A., Jr.; Ruoff, R. S. Chemical Analysis of Graphene Oxide Films after Heat and Chemical Treatments by X-Ray Photoelectron and Micro-Raman Spectroscopy. *Carbon* **2009**, *47*, 145−152.
(9) Li, D.; Müller, M. B.; Gilje, S.; Kaner, R. B.; Wallace, G. G. Processable Aqueous Dispersions of Graphene Nanosheets. *Nat. Nanotechnol.* **2008**, *3*, 101−105.
(10) Stankovich, S.; Dikin, D. A.; Piner, R. D.; Kohlhaas, K. A.; Kleinhammes, A.; Jia, Y.; Wu, Y.; Nguyen, S. T.; Ruoff, R. S. Synthesis of Graphene-Based Nanosheets via Chemical Reduction of Exfoliated Graphite Oxide. *Carbon* **2007**, *45*, 1558−1565.
(11) Pei, S.; Zhao, J.; Du, J.; Ren, W.; Chen, H. Direct Reduction of Graphene Oxide Films into Highly Conductive and Flexible Graphene Films by Hydrohalic Acids. *Carbon* **2010**, *48*, 4466−4474.
(12) Sun, R.; Chen, H.; Li, Q.; Song, Q.; Zhang, X. Spontaneous Assembly of Strong and Conductive Graphene/Polypyrrole Hybrid Aerogels for Energy Storage. *Nanoscale* **2014**, *6*, 12912−12920.
(13) Zhang, X.; Sui, Z.; Xu, B.; Yue, S.; Luo, Y.; Zhan, W.; Liu, B. Mechanically Strong and Highly Conductive Graphene Aerogel and its Use as Electrodes for Electrochemical Power Sources. *J. Mater. Chem.* **2011**, *21*, 6494−6497.
(14) Zhang, J.; Yang, H.; Shen, G.; Cheng, P.; Zhang, J.; Guo, S. Reduction of Graphene Oxide via L-Ascorbic Acid. *Chem. Commun.* **2010**, *46*, 1112−1114.
(15) Nardecchia, S.; Carriazo, D.; Ferrer, M. L.; Gutiérrez, M. C.; del Monte, F. Three Dimensional Macroporous Architectures and Aerogels Built of Carbon Nanotubes and/or Graphene: Synthesis and Applications. *Chem. Soc. Rev.* **2013**, *42*, 794−830.
(16) Sun, H.; Xu, Z.; Gao, C. Multifunctional, Ultra-Flyweight, Synergistically Assembled Carbon Aerogels. *Adv. Mater.* **2013**, *25*, 2554−2560.
(17) Hu, H.; Zhao, Z.; Wan, W.; Gogotsi, Y.; Qiu, J. Ultralight and Highly Compressible Graphene Aerogels. *Adv. Mater.* **2013**, *25*, 2219−2223.
(18) Hong, J. Y.; Bak, B. M.; Wie, J. J.; Kong, J.; Park, H. S. Reversibly Compressible, Highly Elastic, and Durable Graphene Aerogels for Energy Storage Devices under Limiting Conditions. *Adv. Funct. Mater.* **2014**, DOI: 10.1002/adfm.201403273.
(19) Bi, H.; Xie, X.; Yin, K.; Zhou, Y.; Wan, S.; He, L.; Xu, F.; Banhart, F.; Sun, L.; Ruoff, R. S. Spongy Graphene as a Highly Efficient and Recyclable Sorbent for Oils and Organic Solvents. *Adv. Funct. Mater.* **2012**, *22*, 4421−4425.

DOI: 10.1021/acsami.5b00407
ACS Appl. Mater. Interfaces 2015, 7, 6220−6229

(20) Blanco-Fuente, H.; Anguiano-Igea, S.; Otero-Espinar, F. J.; Blanco-Méndez, J. Kinetics of Anhydride Formation in Xerogels of Poly(acrylic acid). *Biomaterials* **1996**, *17*, 1667−1675.
(21) La, Y.; Edwards, E. W.; Park, S.; Nealey, P. F. Directed Assembly of Cylinder-Forming Block Copolymer Films and Thermochemically Induced Cylinder to Sphere Transition: A Hierarchical Route to Linear Arrays of Nanodots. *Nano Lett.* **2005**, *5*, 1379−1384.
(22) Dong, J.; Ozaki, Y.; Nakashima, K. Infrared, Raman, and Near-Infrared Spectroscopic Evidence for the Coexistence of Various Hydrogen-Bond Forms in Poly(acrylic acid). *Macromolecules* **1997**, *30*, 1111−1117.
(23) Qiu, L.; Liu, D.; Wang, Y.; Cheng, C.; Zhou, K.; Ding, J.; Truong, V.; Li, D. Mechanically Robust, Electrically Conductive and Stimuli-Responsive Binary Network Hydrogels Enabled by Superelastic Graphene Aerogels. *Adv. Mater.* **2014**, *26*, 3333−3337.
(24) Qiu, L.; Liu, J. Z.; Chang, S. L. Y.; Wu, Y.; Li, D. Biomimetic Superelastic Graphene-Based Cellular Monoliths. *Nat. Commun.* **2012**, *3*, 1241.
(25) Gibson, L. J.; Ashby, M. F. *Cellular Solids: Structure and Properties*; Cambridge University Press: Cambridge, 1997.
(26) Sun, S.; Wu, P. A One-Step Strategy for Thermal- and pH-Responsive Graphene Oxide Interpenetrating Polymer Hydrogel Networks. *J. Mater. Chem.* **2011**, *21*, 4095−4097.
(27) Shen, J.; Yan, B.; Li, T.; Long, Y.; Li, N.; Ye, M. Mechanical, Thermal and Swelling Properties of Poly(acrylic acid)−Graphene Oxide Composite Hydrogels. *Soft Matter.* **2012**, *8*, 1831−1836.
(28) Huang, Y.; Zeng, M.; Ren, J.; Wang, J.; Fan, L.; Xu, Q. Preparation and Swelling Properties of Graphene Oxide/Poly(acrylic acid-co-Acrylamide) Super-Absorbent Hydrogel Nanocomposites. *Colloid. Surf., A* **2012**, *401*, 97−106.
(29) Lee, S.; Lee, H.; Sim, J. H.; Sohn, D. Graphene Oxide/Poly(acrylic acid) Hydrogel by γ-Ray Pre-Irradiation on Graphene Oxide Surface. *Macromol. Res.* **2014**, *22*, 165−172.
(30) Faghihi, S.; Gheysour, M.; Karimi, A.; Salarian, R. Fabrication and Mechanical Characterization of Graphene Oxide-Reinforced Poly (acrylic acid)/Gelatin Composite Hydrogels. *J. Appl. Phys.* **2014**, *115*, 083513.
(31) Li, R.; Chen, C.; Li, J.; Xu, L.; Xiao, G.; Yan, D. A Facile Approach to Superhydrophobic and Superoleophilic Graphene/Polymer Aerogels. *J. Mater. Chem. A* **2014**, *2*, 3057−3064.
(32) Bi, H.; Xie, X.; Yin, K.; Zhou, Y.; Wan, S.; Ruoff, R. S.; Sun, L. Highly Enhanced Performance of Spongy Graphene as an Oil Sorbent. *J. Mater. Chem. A* **2014**, *2*, 1652−1656.
(33) Wang, Y.; Yadav, S.; Heinlein, T.; Konjik, V.; Breitzke, H.; Buntkowsky, G.; Schneider, J. J.; Zhang, K. Ultra-Light Nanocomposite Aerogels of Bacterial Cellulose and Reduced Graphene Oxide for Specific Absorption and Separation of Organic Liquids. *RSC Adv.* **2014**, *4*, 21553−21558.

DOI: 10.1021/acsami.5b00407
ACS Appl. Mater. Interfaces 2015, 7, 6220−6229